Transparent $CuInS_2$/PMMA Nanocomposites Luminescent in the Visible and NIR Region

Krzysztof Guguła and Michael Bredol

Fachbereich Chemieingenieurwesen, Fachhochschule Münster, Stegerwaldstraße 39, 48565 Steinfurt, Germany

Reprint requests to Prof. Dr. Michael Bredol. Fax: +49-02551962711.
E-mail: bredol@fh-muenster.de

Z. Naturforsch. **2014**, *69b*, 217 – 223 / DOI: 10.5560/ZNB.2014-3264
Received September 18, 2013

Nanocomposites combining functional nanoparticles and transparent polymers allow for stabilization of filler properties over long periods of time while retaining transparency of the polymer matrix. Here we employ $CuInS_2$/ZnS quantum dots (QDs), ternary visible- and NIR-emitting semiconductors as wavelength-tunable luminescent fillers. Luminescence in the near infrared (NIR) is of particular interest in medicine which allows deep penetration into human tissue enabling *in vivo* diagnostics and treatment, while visible emitters may serve as color converters in displays or lighting. To stabilize the optical properties of QDs and prevent agglomeration, polymethyl metacrylate (PMMA) was chosen as a matrix. These novel polymer nanocomposites (PNCs) show good optical properties and stability under ambient conditions, and can be easily deposited over large areas. High-quality QDs and hydrophobic functionalization with long-chain hydrocarbons are a prerequisite for embedding into a PMMA matrix. Transparent PNC films without visible scattering losses were obtained for 1 wt-% QD loading with respect to the polymer. Partial transparency is retained up to 10 wt-% QD loading and vanishes rapidly at higher loading. Luminescence properties increase up to 5 wt-% and then decrease rapidly due to QD agglomeration and reabsorption between adjacent particles. Potential applications include converter materials for medical applications, laser layers, displays and white LEDs.

Key words: Nanocomposite, Color Converter, Luminescence, $CuInS_2$, Quantum Dots

Introduction

Transparent quantum dot/polymer nanocomposites show promising applications as sensor materials [1], light converters in LEDs [2, 3] and quantum cutting layers for solar cells [4]. Immobilizing inorganic nanoparticles in a polymeric matrix allows combining their unique optical [5], electrical, magnetic [6], and thermal [7] properties with the feasibility of polymers while overcoming their tendency towards agglomeration in solution. With particle sizes below *ca.* 40 nm, scattering of light is suppressed [8], thus allowing high levels of transparency. While polymer nanocomposites (PNCs) incorporating *i. e.* CdSe [9], doped Zn(S,Se) nanoparticles [10] or organic dyes [11] are well established for use across the visible spectrum, materials for the near-infrared (NIR) portion of light still have remained largely unexplored. Most of the existing NIR-emitting materials contain toxic elements which are not acceptable in consumer goods.

Luminescent semiconducting nanoparticles cover emission wavelengths from the near-UV to mid-IR [12]. The NIR portion of light is of particular interest in medicine where living tissue does not absorb strongly anymore in the so-called *in vivo* windows, the first of which is located between 670 and 900 nm [13]. To make this region accessible for excitonic luminescence, a semiconductor must have a band gap of approximately 1.8 eV or lower. At such low energy values, carrier relaxation due to lattice vibrations becomes significant, and luminescence is strongly quenched at room temperature. Phonon quenching can be overcome by spatially confining the electrons and holes of a particle to dimensions lower than their Bohr exciton radius,

thus bringing it to a quantum-confined state. Quantum dots are confined in all dimensions and feature size-dependent optical properties.

Among luminescent materials, I-III-VI semiconductors combine high quantum yield, wavelength tunability in the visible and NIR region, broad excitation and emission spectra, and low inherent toxicity. In particular, $CuInS_2$ (CIS) is a notable ternary semiconductor with a bulk band gap of 1.5 eV and an exciton Bohr radius of 4 nm. The emission can be tuned from green for the smallest nanocrystals up to *ca.* 830 nm [14 – 16]. Zhong *et al.* [17] developed the synthesis of highly luminescent CIS QDs by thermolysis of cationic precursors in the presence of excess 1-dodecanethiol (DDT) that acts as a surfactant, complexing agent and sulfur source rendering the QDs inherently p-type with a hydrophobic surface functionalization. Quantum yields as high as 70 % for ZnS-coated particles [18] have been reported up to date. Type I shell alignment with wide band-gap ZnS provides stability against chemical and photodegradation.

Although there has been significant progress in the application of I-III-VI semiconductors [19], most of the research efforts on $CuInS_2$ QDs focused on their potential for solar energy conversion and bio-imaging. CIS-polymer nanocomposites have not been widely studied so far motivating the research efforts presented here.

Experimental Section

$CuInS_2$/ZnS synthesis

Synthesis of CIS/ZnS quantum dots was adopted from earlier reports [17, 20] and modified for increased reaction yield. All precursors were obtained from Sigma-Aldrich and were of analytical grade. All solvents (technical grade) used were obtained from Sigma-Aldrich and used without further purification. The DDT to CuI precursor molar ratio was kept at approximately 40 : 1. Indium acetate ($In(OAc)_3$) and copper iodide (CuI) were used in stoichiometric amounts. The non-coordinating solvent 1-octadecene (ODE) was used as dilutant. The mixture was degassed in vacuum before heating and backfilled with argon several times. QD samples emitting at 570 (QD570) and 590 nm (QD590) were synthesized by injecting the sulfur precursor at 130 and 150 °C, respectively, and annealing for 20 min in DDT and ODE. The sulfur precursor was prepared by dissolving sulfur powder in a 1 : 1 mixture of oleic acid and ODE. 620 (QD620) and 660 nm (QD660) emitters were synthesized by the pyrolysis of DDT at 200 °C for 40 and 90 min, respectively. Shell growth was carried out at 180 °C under argon by drop-wise addition of zinc stearate or zinc acetate ($ZnSt_2$; $Zn(OAc)_2$) in ODE and tri-*n*-octylphosphine sulfide (TOPS, *ca.* 2 : 1 TOP : S) over 15 min. $Zn(OAc)_2$ was used to produce QD570 and QD590 at molar excess of 6 : 1 for Zn : In. $ZnSt_2$ was used to produce QD620 and QD660 at a molar excess of 3 : 1 for Zn : In. Shell precursors were prepared by dissolving sulfur in tri-*n*-octylphosphine under stirring and admixture of $ZnSt_2$ in ODE or $Zn(OAc)_2$ in ODE and oleylamine (OLA) in ambient conditions. QDs were purified by hexane-acetone, chloroform-methanol-acetone and hexane-acetone extraction. Purified QDs were stored in hexane at a concentration of 50 – 150 mg mL^{-1}.

Nanocomposite fabrication

Polymer nanocomposites were prepared by dissolving PMMA granules (Degalan™, Evonik Industries) in toluene at 20 wt-% of PMMA. Next, the concentrated QD solution was added drop-wise into the polymer solution under moderate stirring over several hours. The solution was mildly heated to evaporate hexane and increase viscosity. Stock QD/polymer solutions were prepared and kept stirring in ambient conditions. Luminescent layers were prepared by doctor-blading with initial thickness of *ca.* 100 – 1200 μm and dried under vacuum. 1–15 wt-% PNCs were prepared by spin-coating at 1500 rpm for 60 s and additional samples with 1 – 7.5 wt-% by doctor-blading. All QD loading weight percentages were calculated with respect to dry PMMA.

Characterization

XRD patterns were obtained on a Rigaku Mini Flex II Desktop diffractometer. Particle size was estimated by Dynamic Light Scattering (DLS) on a Malvern Zetasizer NanoXS. Transmittance measurements were conducted using a ThermoScientific Genesys 10S UV/Vis spectrometer. Luminescence properties were assessed on an Edinburgh Instruments FSL900 equipped with a 450 W xenon lamp and a cooled (−20 °C) single-photon counting photomultiplier (Hamamatsu R2658P). The elemental carbon content was measured using an Eltra CS800 analyzer. FE-SEM pictures were taken with a Zeiss-LEO 982 Gemini at 5 kV. Viscosity flow curves were obtained on a Haake Viscotester 550.

Results and Discussion

CIS quantum dots were synthesized and coated with a ZnS shell, a hydrophobic surface and yellow (QD570), orange (QD590), warm red (QD620), or deep red (QD660) emission, with emission peak wavelengths as denoted in parentheses. Samples QD570 and QD590 were synthesized with acetate ligands on

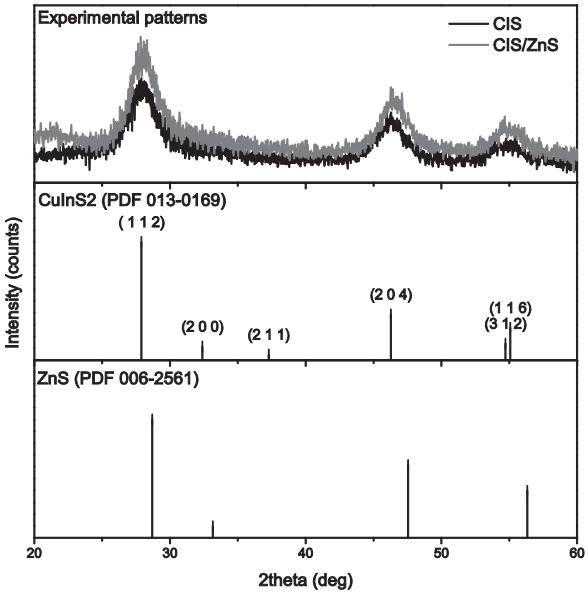

Fig. 1. XRD patterns of CIS and CIS/ZnS with respective chalcopyrite $CuInS_2$ and sphalerite ZnS references.

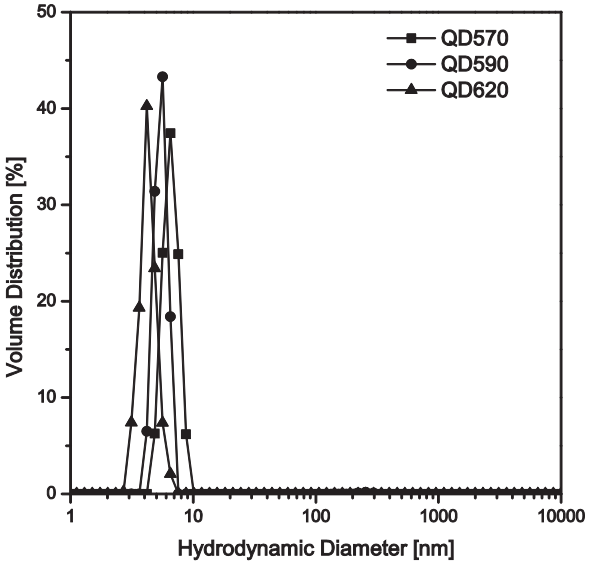

Fig. 2. DLS size distribution of QDs in dilute dispersion by volume.

the zinc ions to facilitate purification procedures under a large excess of zinc precursor, and QD620 and QD660 with stearate ligands. The solvent/antisolvent purification step was crucial for preparing transparent PNCs. Non-polar/polar extractions were meticulously monitored to ensure precipitation of QDs without unreacted precursors. The as-prepared $CuInS_2$ quantum dots exhibited a somewhat low quantum yield of *ca.* 2 – 3 % and agglomerated rapidly while blending with a polymer solution. Overcoating with wide band-gap ZnS stabilized the luminescence to quantum yields of up to 30 % and provided a better interface between CIS/ZnS and PMMA. The XRD pattern of a representative sample revealed broad peaks (Fig. 1) as expected for extremely small particles. All detected peaks can be indexed to the chalcopyrite $CuInS_2$ phase (PDF card no. 013-0169). Coated material exhibited a minor peak shift towards larger angles which proves a successful formation of the ZnS shell with a slightly lower lattice parameter. DLS measurements were conducted to examine the QD behavior in stock solutions. The hydrodynamic diameter was *ca.* 4 – 6 nm as seen in Fig. 2, but due to the presence of long-chain organic ligands, the crystalline core was actually smaller. QD570 and QD590 dots are larger than QD620 due to higher Zn precursor feed resulting in a thicker ZnS shell. Zn ions are suspected to etch the QDs during shell growth effectively, thus decreasing the core size and blue-shifting the luminescence. The QD660 sample could not be measured by DLS due to the laser light being absorbed by the dots. All stock solutions showed no visible agglomeration even after several months in storage. The polymer/QD solutions were stable for at least a week when left without stirring.

Polymer nanocomposites (PNCs) were studied by means of UV/Vis transmittance and photoluminescence (PL). Figure 3a shows the optical properties of PNCs with 1 wt-% QD loading. The transmittance above the QD absorption and emission range is almost as high as that of pure PMMA clearly demonstrating non-agglomerated particles and homogeneous film formation. A 100 μm thick nanocomposite layer with QD620 and QD660 exhibits *ca.* 1 % loss in transmittance with respect to a PMMA layer of the same thickness. Transmittance of QD660 PNC layers with different thicknesses are depicted in an inset in Fig. 3a. Using doctor-blading, layers of up to approximately 110 μm could be easily fabricated. Half of 450 nm blue light intensity can be absorbed with minimal scattering losses making the films potentially useful as color converters from cheap and efficient blue LEDs to NIR. In case of QD570 and QD590 scattering losses are larger presumably due to the short length of the acetate ligands influencing the QD stability in polymer solution.

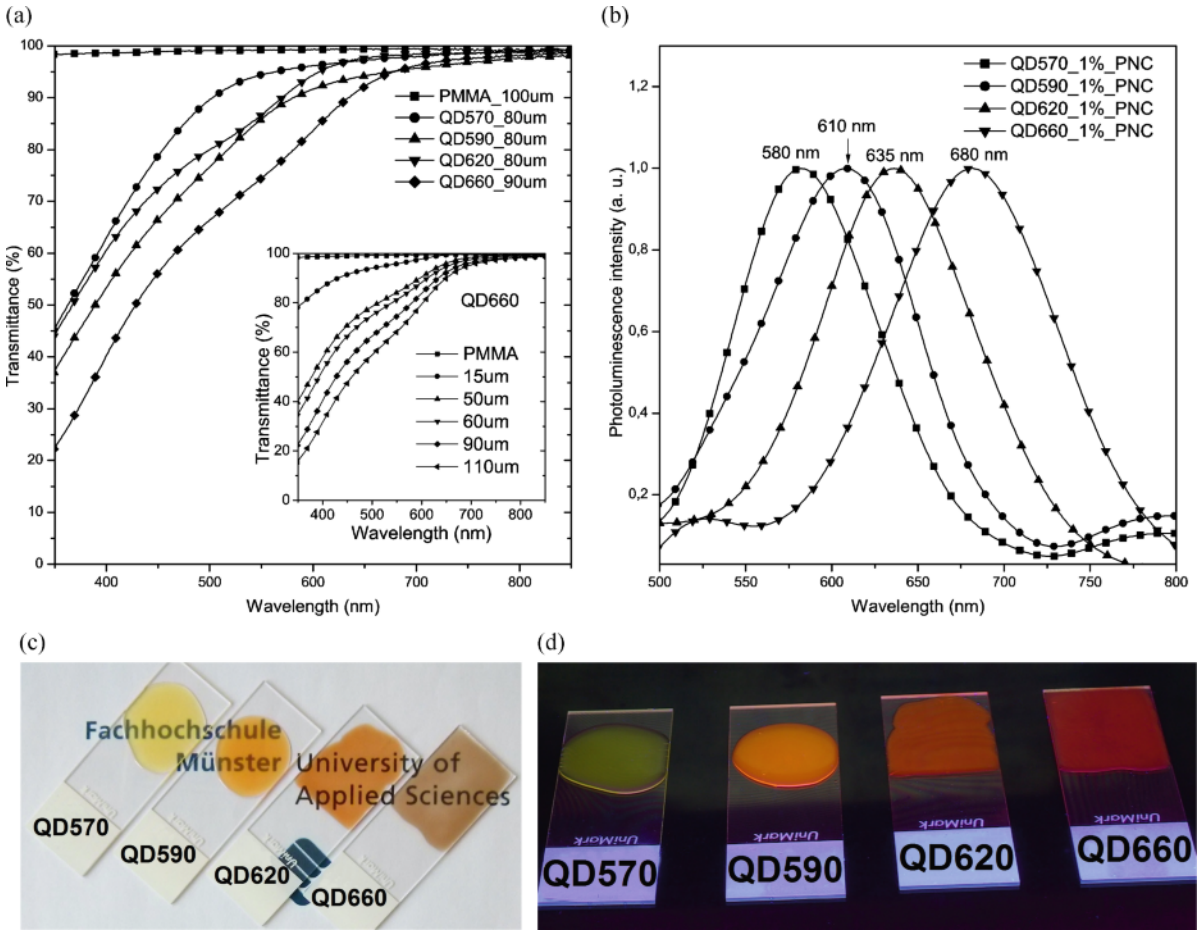

Fig. 3 (color online). Transmittance (a) and luminescence spectra in reflectance setup (b) of 1 wt-% PNCs; the inset shows the transmittance of 1 wt-% QD660 in PMMA with varying layer thickness; view of luminescent PNC layers under ambient light (c) and UV irradiation (d).

QD concentrations higher than ca. 2 wt-% yielded translucent films. Elemental carbon analysis revealed a total organic content of 29 – 33 % in the purified dry QDs. Such a high carbon residue indicates the presence of unbound surfactants. Although small amounts of excess surfactants did not decrease the optical properties of nanocomposites, the presence of unwashed metallic precursors rendered the films translucent regardless of QD loading, as observed in our experiments. Tri-*n*-octylphosphine (TOP) has a high affinity towards oxygen and can bind with PMMA oxygen sites plasticizing the matrix. Adding small amounts of TOP to QD solutions prior to blending with PMMA produced transparent gels that could not be dried.

PNCs prepared with purified QDs, however, did not exhibit plastic behavior after drying. In case of QD570 and QD590 dots, the zinc stearate precursor was replaced with zinc acetate to facilitate the purification procedure. Acetate capped QDs agglomerated rapidly when introduced into the polymer melt above 1 wt-% loading. Luminescence properties of the nanocomposites are red-shifted with respect to samples in dilute dispersion as seen in Fig. 3b. The shift amounts to 10 – 20 nm being larger the bigger the QDs are. Booth *et al.* [21] correlated the $CuInS_2$ particle size with a molar extinction coefficient following a power law dependency. Smaller QDs absorb less incident radiation and therefore reabsorption between adjacent QDs is less prominent. The reabsorption phenomenon thus

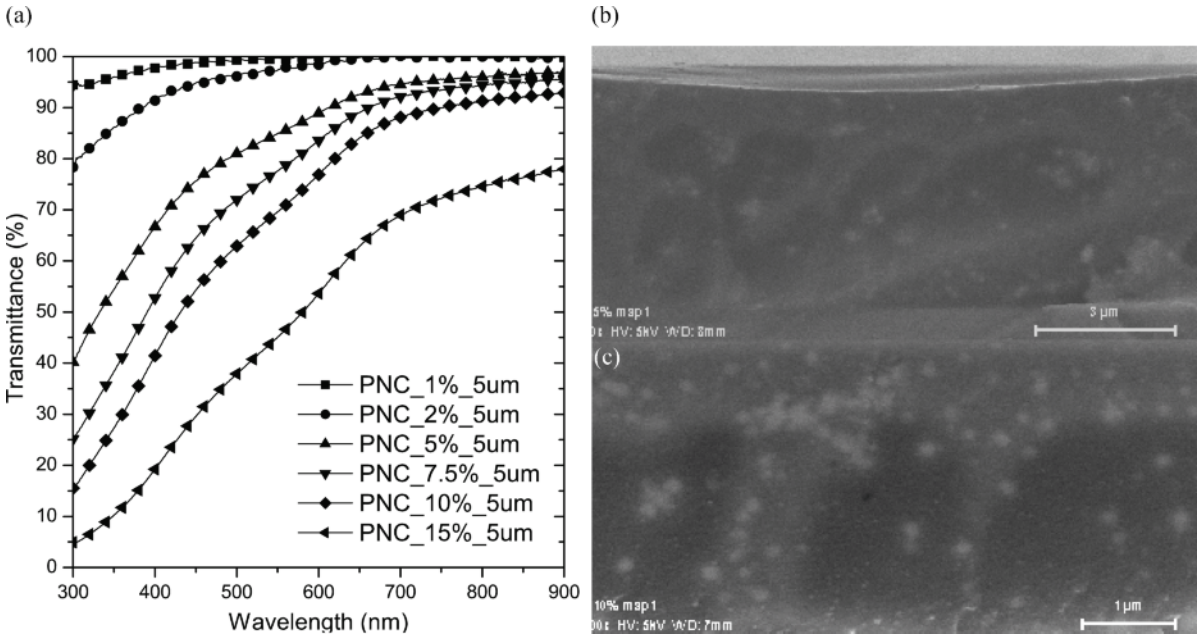

Fig. 4. Transmittance of QD660 PNCs prepared by spin-coating with 1 – 15 wt-% loading (a); cross-section FE-SEM pictures of the corresponding 5 wt-% (b) and 10 wt-% (c) PNCs.

can partially be suppressed by narrowing the particle size distribution. We employed size selective precipitation [22] in an attempt to obtain more monodisperse samples, but to no avail. We observed no apparent change in the shape or position of the luminescence peak. We conclude that while reabsorption is a general phenomenon observed in quantum dots [23], there is more benefit in using ternary I-III-VI QDs as luminescent fillers rather than their binary counterparts for their larger Stokes shift [19] allowing for higher amounts of filler loading before luminescence is quenched.

Optical properties of the PNCs were re-measured periodically and were found to be stable during the 90 d testing period when stored under ambient conditions. The luminescence properties of nanocomposites can be tuned by varying QD growth time and temperature as well as nanocomposite thickness and QD loading. Substituting indium by *e. g.* gallium, or replacing copper by silver, can be used to tune the band gap and expand the luminescence range further into the blue region of the visible spectrum.

We have investigated the influence of filler loading on scattering and luminescence quenching. QD660 dots were employed to fabricate 1 – 15 wt-% PNCs, using spin-coating to exclude the influence of prolonged drying on the properties of the final product. As depicted in the transmittance plot (Fig. 4), two agglomeration stages are revealed with respect to QD loading. Slight scattering begins at 5 – 10 wt-% and becomes very pronounced at 15 wt-%. The transmittance at 800 nm amounts to 96, 94 and 91 % for 5, 7.5 and 10 wt-% QD loading, respectively, and decreases dramatically to 75 % at 15 wt-% loading. Spin-coated nanocomposites were 5 μm thick. FE-SEM investigation revealed the formation of *ca.* 100 nm large agglomerates increasing in size and fusing together at higher loading, thus causing the 15 wt-% PNC to scatter like bulk composites with agglomerates grown larger than the wavelength of visible light. Wang *et al.* [24] found 3-mercaptopropionate-capped $CuInS_2$ QDs to strongly scatter above 10 wt-% loading when embedded in a cellulose matrix. Rapid agglomeration was induced above 10 wt-% (2.5 vol-%) loading matching our findings. While occurring in chemically different matrices, the rapid agglomeration may partially be due to the morphology of $CuInS_2$/ZnS quantum dots. HR-TEM investigations revealed tetrahedrally shaped QDs [16, 20] that possess a larger interface area than corresponding spherical particles.

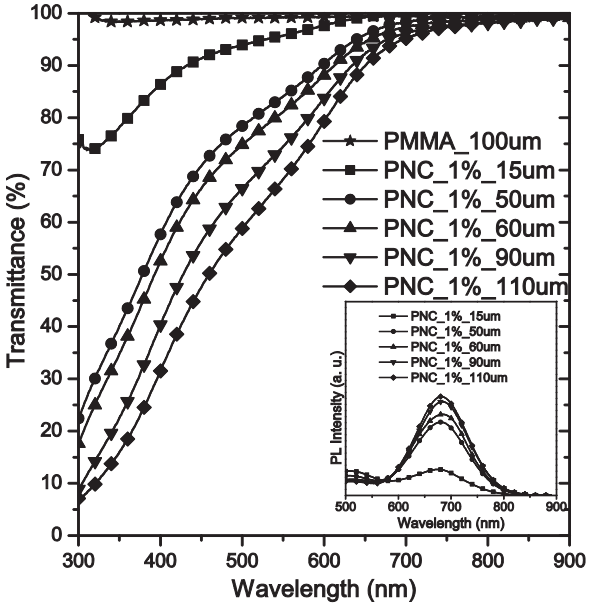

Fig. 5. Emission spectra of QD660 spin-coated PNCs with monochromatic 450 nm excitation in reflectance mode; the inset shows luminescence spectra of stacked doctor-blade samples excited with a blue LED in transmission mode.

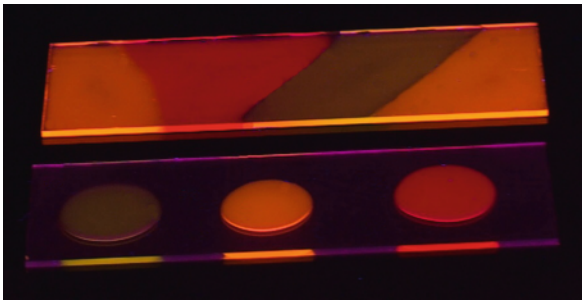

Fig. 6 (color online). Luminescent layer composed of different nanocomposite blends obtained by "painting" on glass and casting 150 μL drops of QD/polymer solutions on soda-lime glass ($d = 10 - 15$ mm).

Emission spectra of spin-coated samples, measured in reflectance mode excited with monochromatic 450 nm light, are depicted in Fig. 5. The emission steadily increases and is almost doubled at 15 wt-% loading when compared to 10 wt-%. The enhancement is due to a higher absorbance of the thin film caused by scattering and an increased number of luminescent centers in the matrix. While scattering is beneficial for some applications, in laser layers it needs to be avoided. An additional 5 – 10 nm peak shift at higher loading indicates increasing reabsorption and luminescence from agglomerates. In turn, the quantum yield of luminescence in 10 – 15 wt-% PNCs is expected to decrease. To compare PNCs performance for color converter applications we have measured the nanocomposites in transmittance mode illuminated by a 1 W blue LED. The inset in Fig. 5 represents stacked QD660 containing doctor-blade samples measured in transmittance mode. The results confirmed our expectations from previous measurements. Transparent samples with 1 – 2 wt-% QDs have a luminescence peak at 680 nm regardless of sample thickness but require a higher optical path length than provided to absorb all incident radiation. The peak in the blue range comes from the PMMA matrix. The strongest luminescence was obtained for 5 wt-% loading with most of the excitation light being absorbed directly or aided by scattering. The peak of luminescence is red-shifted by 20 nm with respect to non-scattering PNCs indicating reabsorption from agglomerates. Increasing the concentration to 7.5 wt-% decreased the luminescence by a factor of 5 and shifted the peak further into the NIR region. The real ratio of the peaks due to $CuInS_2$ and to the matrix was difficult to measure quantitatively owing to problems with the detector sensitivity in the NIR.

Fig. 6 depicts luminescent layers prepared by painting a glass surface using a Pasteur pipette. Multicolored samples can be easily obtained, and special patterns can be realized simply by applying a mask. Room temperature viscosity measurements of 1 wt-% PNC solutions revealed a mostly Newtonian flow up to a shear rate of 500 s^{-1} and η in the range of 200 – 250 mPas. A higher viscosity can be reached by controlled solvent evaporation rather than by increasing the initial polymer concentration in solution to facilitate dispergation of the particles in the liquid. The measured flow properties are suitable for a wide range of application techniques such as printing, dip-coating, spin-coating, painting *etc.* The properties of stock PNC solutions can be further tuned by using high-boiling solvents like ethyl benzoate or low-boiling solvents like tetrahydrofuran. Toluene was used with doctor-blading technique because of its moderate volatility, easy PMMA dissolution, miscibility with hexane and stability of stock PNC solutions. QDs stored in hexane did not undergo degradation and showed no decrease

in quantum yield during storage at room temperature for at least several months.

Conclusion

In summary, $CuInS_2$/ZnS quantum dots were embedded *ex situ* into polymethyl metacrylate matrices with up to 15 wt-% loading. Luminescence intensities increased up to 5 wt-% and decreased rapidly at higher concentrations. Highly transparent nanocomposites were obtained at 1 wt-% loading enabling potential applications as NIR converter layers and thin films for lasing and lighting. Nanocomposite films can be easily fabricated on larger scale using various coating techniques and are stable under ambient conditions. Synthetic and purification procedures for quantum dots were found to a have major influence on the quality of the resulting polymer nanocomposites. Long-chain carboxylates (C_{12}–C_{18}) stabilized the quantum dots in the polymer solution and in solid nanocomposites. Acetate groups with their short chain induced nanoparticle agglomeration in the polymer solution already above 1 wt-% loading.

Acknowledgement

The authors acknowledge financial support from the German Federal Ministry of Education and Research (BMBF) in the framework of the project line "NT". We thank AG Tailored Optical Materials of FH Münster for access to fluorescence and UV/Vis spectrometers as well as useful discussions.

[1] A. Bueno, I. Suárez, R. Abargues, S. Sales, J. P. Martinez-Pastor, *IEEE Sensors J.* **2012**, *12*, 3069 – 3074.
[2] H. Kim, J. Y. Han, D. S. Kang, S. W. Kim, D. S. Jang, M. Suh, A. Kirakosyan, D. Y. Jeon, *J. Crystal Growth* **2011**, *326*, 90 – 93.
[3] Y. Yuan, M. Krüger, *Polymers* **2012**, *4*, 1 – 19.
[4] H. Gordillo, I. Suárez, P. Rodríguez-Cantó, R. Abargues, R. García-Calzada, V. Chyrvony, S. Albert, J. Martínez-Pastor, *Proc. SPIE* **2012**, *8424*, 84242A-1.
[5] S. Hoogland, V. Sukhovatkin, I. Howard, S. Cauchi, L. Levina, E. H. Sargent, *Opt. Express* **2005**, *14*, 3273 – 3281.
[6] P. Sun, H. Zhang, C. Liu, J. Fang, M. Wang, J. Chen, J. Zhang, C. Mao, S. Xu, *Langmuir* **2010**, *26*, 1278 – 1284.
[7] Y. Deng, A. Gu, Z. Fang, *Polym. Int.* **2004**, *53*, 85 – 91.
[8] H. Althues, J. Henle, S. Kaskel, *Chem. Soc. Rev.* **2007**, *36*, 1454 – 1465.
[9] X. Zhong, R. Xie, Y. Zhang, T. Basche, W. Knoll, *Chem. Mater.* **2005**, *17*, 4038 – 4042.
[10] N. Pradhan, D. D. Sarma, *J. Phys. Chem. Lett.* **2011**, *2*, 2818 – 2826.
[11] U. Resch-Genger, M. Grabolle, S. Cavaliere-Jaricot, R. Nitschke, T. Nann, *Nature Meth.* **2008**, *5*, 763 – 775.
[12] I. L. Medintz, H. T. Uyeda, E. R. Goldman, H. Mattoussi, *Nature Mater.* **2005**, *4*, 435 – 446.
[13] R. Weissleder, *Nature Biotechn.* **2001**, *19*, 316 – 317.
[14] L. Li, T. J. Daou, I. Texier, T. T. K. Chi, N. Q. Liem, P. Reiss, *Chem. Mater.* **2009**, *21*, 2422 – 2429.
[15] D. Deng, Y. Chen, J. Cao, J. Tian, Z. Qian, S. Achilefu, Y. Gu, *Chem. Mater.* **2012**, *24*, 3029 – 3037.
[16] W. Guo, N. Chen, Y. Tu, C. Dong, B. Zhang, C. Hu, J. Chang, *Theranostics* **2013**, *3*, 99 – 108.
[17] H. Zhong, Y. Zhou, M. Ye, Y. He, J. Ye, C. He, C. Yang, Y. Li, *Chem. Mater.* **2008**, *20*, 6434 – 6443.
[18] Y. K. Kim, S. H. Ahn, K. Chung, Y. S. Cho, C. J. Choi, *J. Mater. Chem.* **2012**, *22*, 1516 – 1520.
[19] H. Zhong, Z. Bai, B. Zou, *J. Phys. Chem. Lett.* **2012**, *3*, 3167 – 3175.
[20] L. Li, A. Pandey, D. J. Werner, B. P. Khanal, J. M. Pietryga, V. I. Klimov, *J. Am. Chem. Soc.* **2011**, *133*, 1176 – 1179.
[21] M. Booth, A. P. Brown, S. D. Evans, K. Critchley, *Chem. Mater.* **2012**, *24*, 2064 – 2070.
[22] C. B. Murray, D. J. Norris, M. G. Bawendi, *J. Am. Chem. Soc.* **1993**, *115*, 8706 – 8715.
[23] B. C. Mei, J. Wang, Q. Qiu, T. Heckler, A. Petrou, *Appl. Phys. Lett.* **2008**, *93*, 083114.
[24] H. Wang, Z. Shao, B. Chen, T. Zhang, F. Wang, H. Zhong, *RSC Advances* **2012**, *2*, 2675 – 2677.